Science Advances
AAAS

advances.sciencemag.org/cgi/content/full/5/1/eaav1887/DC1

Supplementary Materials for

Monsoon-driven Saharan dust variability over the past 240,000 years

C. Skonieczny*, D. McGee, G. Winckler, A. Bory, L. I. Bradtmiller, C. W. Kinsley, P. J. Polissar, R. De Pol-Holz, L. Rossignol, B. Malaizé

*Corresponding author. Email: charlotte.skonieczny@u-psud.fr

Published 2 January 2019, *Sci. Adv.* **5**, eaav1887 (2019)
DOI: 10.1126/sciadv.aav1887

This PDF file includes:

Supplementary Material and Methods

Age model

$\delta^{18}O_{ben}$ data from ODP659 were used to develop an age model over the last 5 Myr (*3*). The stratigraphy of core MD03-2705 core covering the last 240 ka is based on ^{14}C dating and $\delta^{18}O_{ben}$ data (*13*, *24*, *50*). In this study, nine new radiocarbon dates as well as three new benthic $\delta^{18}O_{ben}$ tie points were added to improve the age model (table S1). The AMS-^{14}C dates were obtained on monospecific samples of planktonic foraminifera *G. bulloides* at the Keck AMS facility of the University of California at Irvine. AMS-^{14}C dates were calibrated into calendar years using the software CALIB 6.0 (*51*) using a surface reservoir age of 478 years (mean age surface reservoir for West African sites (*51*)) and the Marine13 calibration curve. Beyond the range of AMS-^{14}C ages, the age model is based on the correlation of the $\delta^{18}O_{ben}$ record (*P. wuellerstorfi*) (*25*) with the $\delta^{18}O_{ben}$ LR04 Stack (*50*, *52*). We have chosen to remove some $\delta^{18}O_{ben}$ tie points from (*50*) and added 3 new $\delta^{18}O_{ben}$ tie points over the last 100 ka obtained from a $\delta^{18}O_{ben}$ composite record from the Iberian margin, which presents a high-resolution record tied to Greenland ice core chronologies (*53*). All tie points of the new age model are presented in table S1. From 0 to 198 cm, 3 polynomial regressions were used to create the age model for the last 27 ka in order to best fit the tie points (fig. S1), and a piecewise linear age model was used for the remainder of the last 240 ka (fig. S1).

Mass accumulation rates

The canonical North African Plio-Pleistocene dust record from ODP659 is based on terrigenous (i.e., non-carbonate) percentages and age model-based MARs (*3*). In calculating MARs, linear sedimentation rates (LSRs) are first derived from an age model based on benthic $\delta^{18}O$ and magnetic data (*3*). LSRs are then multiplied by dry bulk densities (DBDs) measurements to calculate MARs. Dust MARs are then

calculated by multiplying higher-resolution terrigenous percent data by bulk MARs (*3*). DBDs, dust percentages, LSRs and MARs data from ODP659 over the last 240 ka are presented in fig. S2.

The use of this approach to determine dust fluxes has two primary sources of potential bias. First, age model-based MARs measure total sediment accumulation and integrate lateral and vertical sedimentary inputs to the core site. Changes in lateral sediment advection can thus create spurious dust flux changes. Second, because age model tie points occur at about 20 ka intervals for the ODP659 record (*3*), dust MARs are in reality limited to this resolution. Multiplying a low-resolution MAR by higher-resolution terrigenous percent data to produce a higher resolution dust flux record assumes that changes in terrigenous percent are driven solely by changes in dust flux. However, short-term terrigenous percent changes may also be driven by variations in biogenic sediment contents, for example due to calcium carbonate dissolution.

In order to compare the eolian signals recorded by ODP659 and MD03-2705, we have calculated MARs for MD03-2705 over the last 240 ka (fig. S2). MD03-2705 dust percentages (fig. S2) are calculated as non-carbonate sediments for consistency with the methods used for ODP659, with $CaCO_3$ percentage obtained by coulometry (see below for details) (table S2). Biogenic opal percentages are low at this site (2.7±1.1% over the last 240 ka; L. Bradtmiller, unpublished data), and so neglecting opal does not substantially affect dust percentages. As no DBD measurements exist for the MD03-2705 core, DBDs were estimated by the empirical relationship proposed for the equatorial Atlantic (*54*) (fig. S2) using the following equation

$$DBD\ (g.cm^{-3}) = 0.0066 \times (\%\ CaCO_3) + 0.29 \qquad (1)$$

In order to compare the same parameters, ODP659 DBDs were also estimated using this empirical relationship for the last 240 ka (fig. S2). Measured (*3*) and estimated (this study) DBD are within the same range but present differences in their variability through the last 240 ka (fig S2). MD03-2705 LSRs (fig. S2) were calculated using tie points presented in fig. S1 and table S1. Finally, MD03-2705 dust MARs (fig. S2) were calculated as described before for ODP659.

ODP659 and MD03-2705 dust percentages are very similar, confirming that these two neighboring sites register the same eolian signal (fig. S2). LSRs are within the same range (~ 5 cm/ka), with higher millennial-scale variability at MD03-2705 likely due to its higher-resolution age model. ODP659 MARs obtained from measured (*3*) and estimated (this study) DBDs are quite similar (fig. S2, Panel D) indicating that DBD changes are not the main driver of MAR variability.

Dust MARs are higher and show more high-frequency variability at MD03-2705 than at ODP659 due to the differences in mean LSR and age model resolution between the sites, though the two sites have similar variability at 10^4-year timescales (fig. S2). This observation is supported by the spectral analysis conducted on dust MARs and dust percentages for both sites (Fig. 2 and fig. S3). The higher-resolution age model of MD03-2705 creates LSR and thus MAR records with prominent short-term peaks, smearing the spectral signal of the MD03-2705 dust MAR record when compared to the power spectrum of ODP659 dust MAR (fig. S3), but still showing the concentration of power at timescales greater than that of precession. In the context of this study, a more central comparison is between the spectra of the dust percentage records (Fig. 2), as they are of comparable resolution, and because dust percentages vary much more on orbital frequencies than the other contributors to MAR calculations (LSR and DBD) and

are thus the dominant contributor to orbital-scale dust MAR variability.

Benefits of ^{230}Th-normalization

^{230}Th-normalization has several key advantages over age model-based MARs. First, as discussed in the main text, age model-based MARs are limited by the resolution and accuracy of the age model. For ODP659 (and most sites with MAR records spanning multiple glacial-interglacial cycles), the time between age model tie points averages ~20 ka (*3*), limiting age model-based fluxes to this resolution. When higher-resolution dust percentage and density data are multiplied by age model-based sedimentation rates to produce dust MARs at the resolution of the dust percentage data, the assumption is made that sedimentation rates are constant between age model tie points, and that changes in dust percentage are due to changes in dust supply, not changes in the supply or preservation of biogenic components of the sediment (chiefly carbonate.) For ^{230}Th-normalization, sedimentary accumulation rates are determined for each depth at which U and Th isotopes are measured, allowing the construction of high-resolution dust flux records. For these records, short-term changes in biogenic supply or preservation will be evident in biogenic and total sediment accumulation rates, reducing potential biases due to changes in carbonate dissolution. ^{230}Th normalization is also largely insensitive to age model errors or low age model resolution, unlike age model-based MARs.

Second, age model-based fluxes measure total accumulation at the site, integrating sedimentary inputs from both sinking particles and laterally redistributed sediments. Fluxes may then be biased by changes in lateral sediment redistribution independent of changes in vertical sediment inputs. ^{230}Th-normalization accounts for lateral inputs and produces a more accurate estimate of vertical sediment inputs, as redistributed sediments have similar adsorbed ^{230}Th concentrations to sediments sinking

through the overlying water column. Previous studies have found that ^{230}Th-normalized estimates are able to produce high-fidelity estimates of vertical rain rates for clay- and silt-sized fractions of the sediment even in sites with high amounts of lateral sediment redistribution (*55–58*).

Dust and carbonate flux calculations and uncertainties

Following calculation of bulk ^{230}Th-based sediment fluxes, the accumulation rates of dust, $CaCO_3$ or other sedimentary components can be calculated by multiplying the fraction of a given component by the bulk ^{230}Th-normalized sediment flux. Dust percentages for the ^{230}Th-normalized dust flux record were calculated from measured ^{232}Th concentrations and the assumption that ^{232}Th concentrations in dust deposited at the site are 11 µg/g, a value appropriate for the modal grain size of the terrigenous fraction of these samples (~10 µm) (*59*). This value produces the same average terrigenous percentage as that calculated from the residual after biogenic sediments (calcium carbonate, biogenic opal, and organic matter) have been removed, but it has the advantage that ^{232}Th is measured in the same aliquot for which fluxes are determined. In this approach, the terrigenous fraction of the sediment is assumed to be primarily eolian. As detailed above, this assumption is supported by the core's distance from the coast, its location on a local bathymetric high, and its location under the core of the Saharan dust plume. We assign a nominal 5% 1-sigma uncertainty to the estimated eolian fraction of the sediment to account for uncertainties in this assumption and in the ^{232}Th concentration of eolian dust.

The remaining uncertainty in reconstructed dust fluxes stems from uncertainties in the ^{230}Th-normalized bulk sediment fluxes, as described above. These uncertainties reflect corrections for ^{230}Th associated with detrital grains and authigenic uranium and increase with increasing age and detrital content. Eleven replicate aliquots were analyzed for samples between 661-991 cm (~115-183 ka), with an average

difference in dust fluxes between replicates of 13%. Four replicates were also analyzed for samples in the upper 124 cm of the core (6-18 ka) to test reproducibility between MIT and UBC. The mean difference in dust fluxes was 6%, indicating good agreement between the two labs. The smaller value relative to within-lab replicates reflects the fact that the importance of corrections for supported ^{230}Th becomes greater with increasing age, and all samples processed for intra-lab reproducibility were substantially older than those tested for inter-lab reproducibility. For samples with replicates, the error-weighted mean and its uncertainty were used in the final dust flux record.

Uncertainties for dust fluxes do not reflect uncertainties in the assumption that the supply of ^{230}Th to the sediment is equal to its production rate in the overlying water column. Modeling and sediment trap studies suggest that this assumption is correct to within 30% in most sedimentary environments (*20, 43, 60*) with departures of only ~40% even in the Mauritanian upwelling region to the east of our core site, an area with strong gradients in Th scavenging (*61*). Moreover, offsets between water column production and the vertical rain of ^{230}Th are likely to remain relatively constant downcore if sedimentation regimes remain similar through time (*62*), making the uncertainty in relative changes in accumulation rates–the focus of the present study– substantially smaller than 30%.

Impact of the dust flux uncertainties on the power spectral analysis

In order to evaluate the impact of the uncertainty in the ^{230}Th-normalized dust fluxes on the power spectral analysis, we conducted power spectral analysis on the ^{230}Th-normalized dust fluxes after adding 1-sigma uncertainties and then after subtracting 1-sigma uncertainties. Because uncertainties (both absolute and relative) generally increase with increasing dust fluxes, adding 1-sigma uncertainties increases the amplitude of dust flux variations, while subtracting 1-sigma uncertainties minimizes this

amplitude. The 23-ka signal remains larger than the 100- and 41-ka signals with either adding or subtracting 1-sigma uncertainties (fig. S4).

Supplementary Text

Drivers of observed changes in Saharan dust emissions

Here we examine the potential drivers of dust emission changes in order to assess the connection between dust fluxes at our core site and regional monsoon strength. There are three potential drivers of orbital- and millennial-scale changes in winter dust emissions from the Sahara: the supply of fine-grained material, aridity, and surface winds.

The supply of fine-grained material in dust source regions has been mentioned as a contributing factor in past dust emission changes by some authors (*63*), but several observations suggest that it is of minor importance. First, very high dust deposition is observed in Heinrich Stadial 1 at the end of the last glacial period (e.g., core GC68 on the NW African margin (*22*)). This peak in dust deposition occurs after a prolonged period of dry conditions in the Sahara, over 30 ka after the most recent humid period at ~55 ka (*17*). Second, dust emissions have been gradually rising over the last 5 ka following the end of the African Humid Period (*21–23*); if supply were the primary control, dust emissions should peak immediately following the humid period and then diminish. Finally, modern observations suggest that fine-grained material can be generated by wind abrasion of sand grains, indicating that precipitation is not required to produce fine grains for long-range transport (*64*).

A second driver of past dust emission changes is aridity. Reduced precipitation decreases soil moisture and vegetation density, enabling increased dust emissions. Modeling studies seeking to simulate

Holocene changes in dust deposition observed in sediment cores have emphasized the importance of soil moisture and vegetation density in decreasing dust emissions during the Green Sahara period of the Early and mid-Holocene (*8*, *65–67*). This mechanism is certain to be important in reducing dust emissions during humid periods, but it may only be important during climates wetter than today. Modern decadal variations in dust emissions from the Sahara are controlled by surface wind strength rather than precipitation or vegetation density (*68*, *69*), and it is not likely that periods of reduced summer insolation relative to today (e.g. MIS5d, ~115 ka) would have significantly expanded dust source areas in northwest Africa, the source region for MD03-2705 (*70*, *71*), as this region is already arid under modern conditions.

A final potential driver of past dust emission changes is surface winds. As mentioned above, winds are the primary driver of recent decadal variations in dust emissions from the Sahara (*68*, *69*). On millennial and orbital timescales, the covariation of proxies for wind-driven upwelling and dust deposition supports winter trade winds as an important driver of dust emission changes from northwest Africa (*7*, *21*, *22*, *72*). In modern observations, interannual variations in dust-generating winds vary with the position of the regional Intertropical Convergence Zone (ITCZ), strengthening in years in which the ITCZ is displaced farther south than normal (*68*). This relationship results from anomalously high pressures over the Sahara in years in which the near-surface convergence in West Africa is displaced south, setting up northeasterly winds that drive dust emissions (*6*, *68*). During "Green Sahara" periods (precessional maxima in summer insolation), model simulations suggest that northeasterly winds weakened in both winter and summer in association with anomalously low surface pressures over the Sahara (*8*). During precessional minima in local summer insolation (e.g. MIS 5d), simulations suggest that the regional ITCZ was displaced anomalously far south in both summer and winter (*73*). Coherent variations in

summer and winter surface pressures and winds over the Sahara in response to orbital and millennial-scale forcings are supported by dust flux records spanning the last 20 ka, which show similar signals in sites reflecting summer and winter dust deposition (*23*).

Together, these findings suggest that West African monsoon rainfall and surface winds vary coherently on a wide range of timescales. As a result, efforts to isolate aridity versus wind strength as controls on long-term dust emissions may be misplaced, and dust—even in winter—acts as an integrated tracer of monsoon strength.

Deep Atlantic [CO_3^{2-}] reconstructions and carbonates fluxes

Deep Atlantic carbonate ion concentration ([CO_3^{2-}]) reconstructions have the greatest spatial coverage during the last glacial inception (~90-50 ka), so our comparison focuses on this period. [CO_3^{2-}] values in the equatorial and northeastern Atlantic at depths of 3-5 km declined between 80 and 65 ka (*27*), implying more corrosive waters at this time. $CaCO_3$ fluxes at MD03-2705 (3085 m water depth) decrease at the same time (fig. S5), suggesting control of $CaCO_3$ burial fluxes by $CaCO_3$ dissolution.

Power spectral analysis was calculated for the ^{230}Th-normalized $CaCO_3$ fluxes and clearly indicates a 41-ka frequency as primary orbital forcing (Fig. 2), indicating that biogenic $CaCO_3$ deposited at the MD03-2705 site (and ODP659 by extension) is mainly driven by high-latitude changes rather than local summer insolation, in contrast with dust ^{230}Th-normalized dust fluxes.

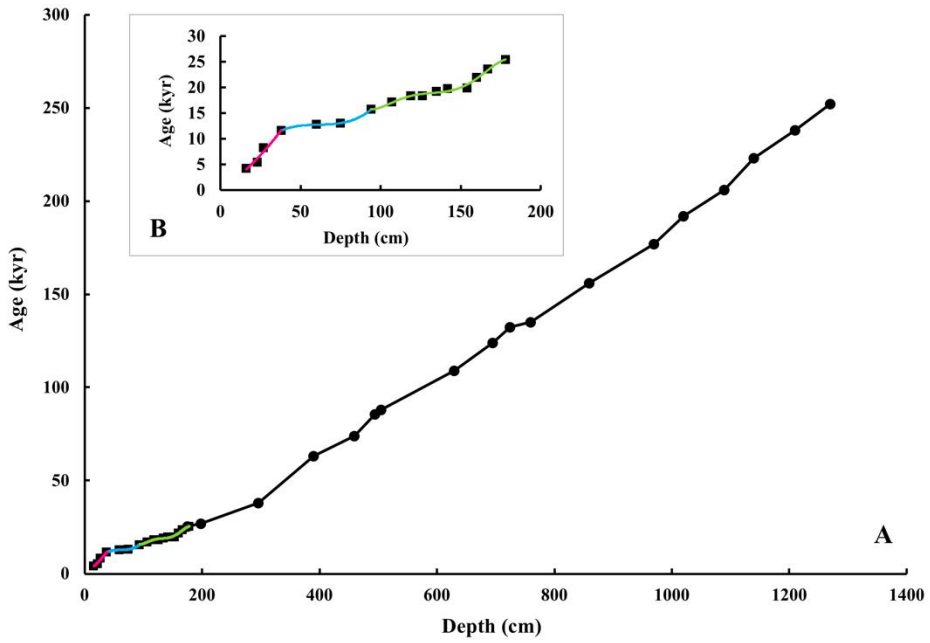

Fig. S1. MD03-2705 age model for the past 240 ka. AMS-^{14}C dates are represented by black squares and $^{18}\delta O_{ben}$ tie points are represented by black dots (see table S1 for details). From 198 to 1270 cm, the calculated linear regression is represented by the black curve of the main panel (**A**). The 3 polynomial regressions calculated for the last 198 cm (order 2 in pink, order 3 in blue and order 5 in green) are enlarged in panel (**B**).

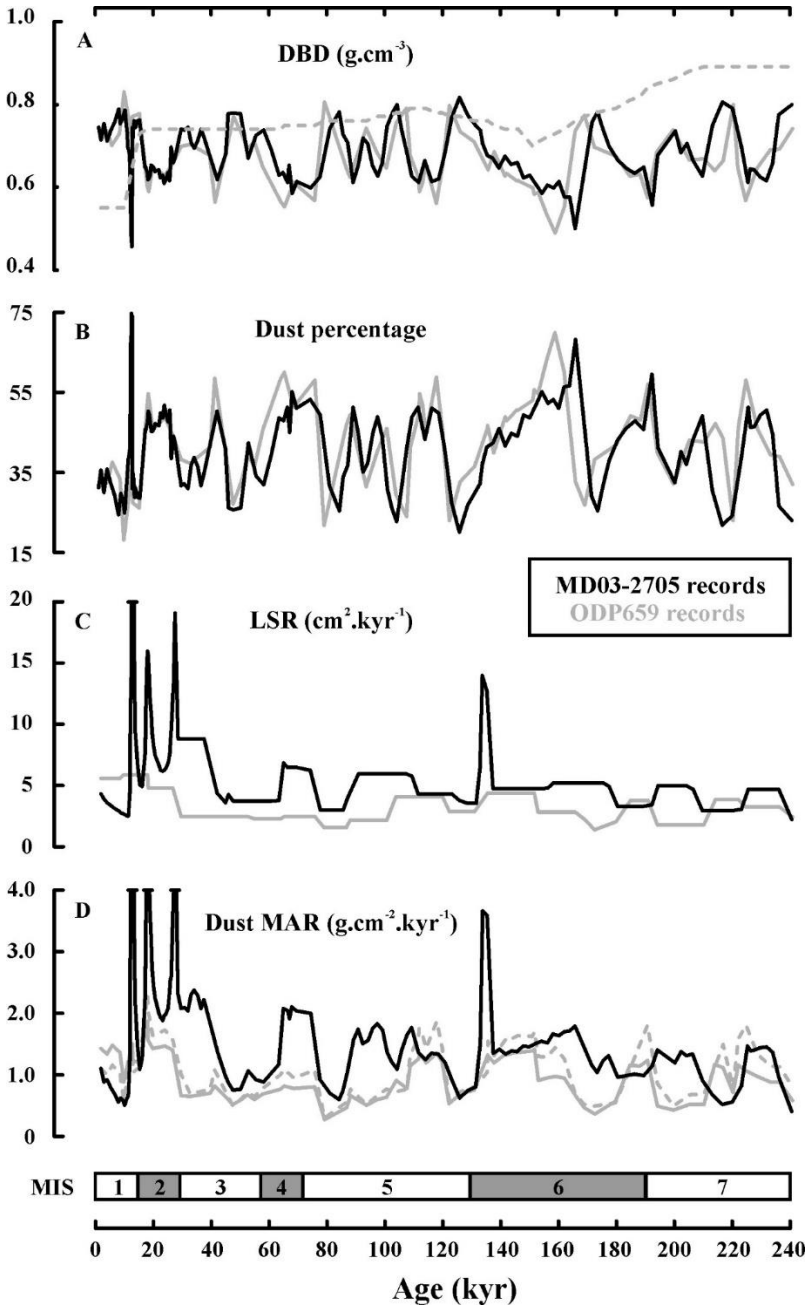

Fig. S2. Sedimentological parameters used in the dust MAR calculation for MD03-2705 and ODP659 for the past 240 ka. MD03-2705 (black) and ODP659 (grey) dry bulk density (DBD) (**A**), dust percentage (**B**), linear sedimentation rates (**C**) and dust mass accumulation rates (MARs) (**D**) for the last 240 ka. ODP659 dashed lines correspond to DBD and MAR calculated with discrete DBD measurements (*3*), whereas solid lines reflect DBD estimated using the empirical equation of (*54*).

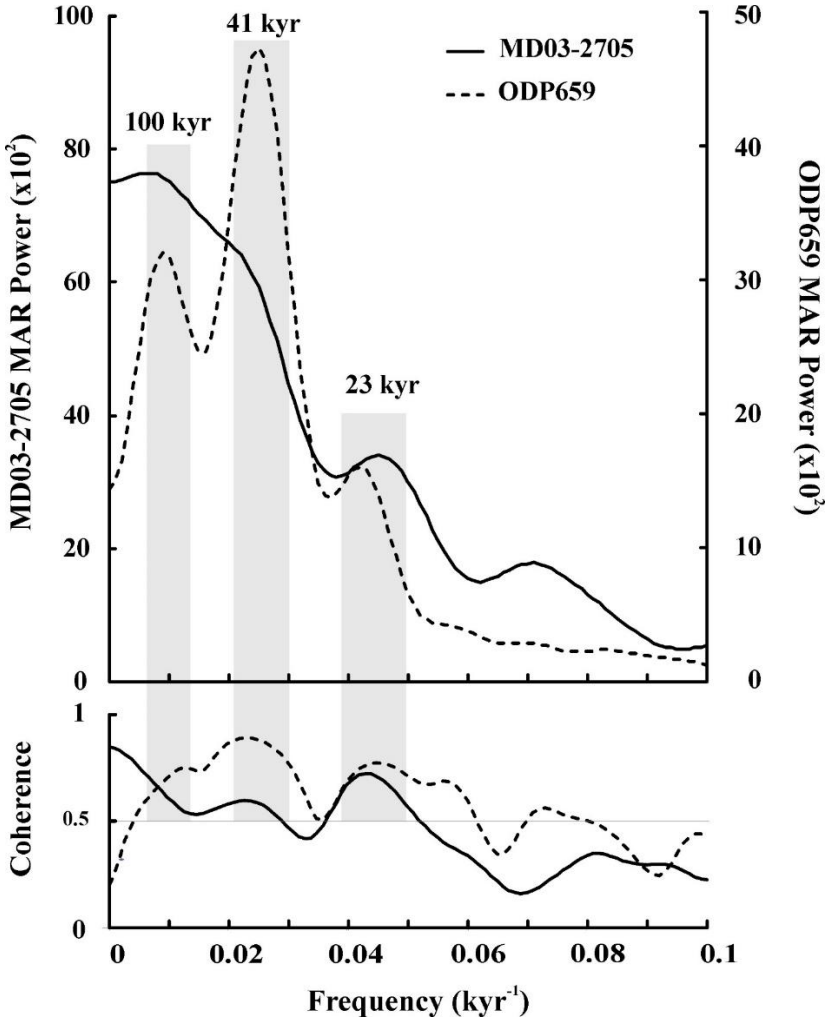

Fig. S3. Power spectral analysis of MD03-2705 and ODP659 dust MARs. Power spectral analyses (top panel) and associated coherences (bottom panel) for MD03-2705 (black) and ODP659 (dashed line) dust MARs. Grey bars highlight the main orbital cyclicities (100, 41 and 23 ka) for which a peak in power variance is associated with a coherence higher than 0.5.

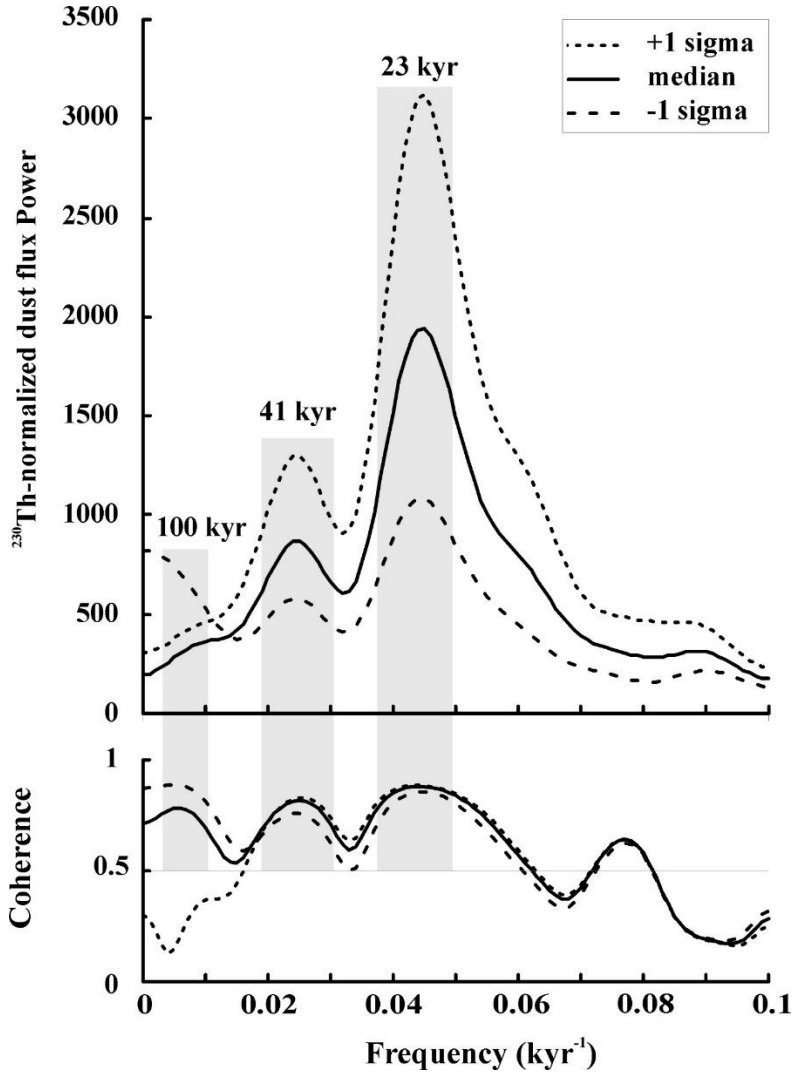

Fig. S4. Power spectral analysis of MD03-2705 ^{230}Th-normalized dust flux records at the extremes of 1-σ uncertainties. Spectral analyses have been conducted on the ^{230}Th-normalized dust flux including both the highest and the lowest uncertainties (± 1sigma) in order to show the lower and greater amplitude variability of the spectra. All spectral analyses indicate that the precessional 23-ka cyclicity remains larger than the 100- and 41-ka signals in the dust fluxes with either +1sigma or -1sigma.

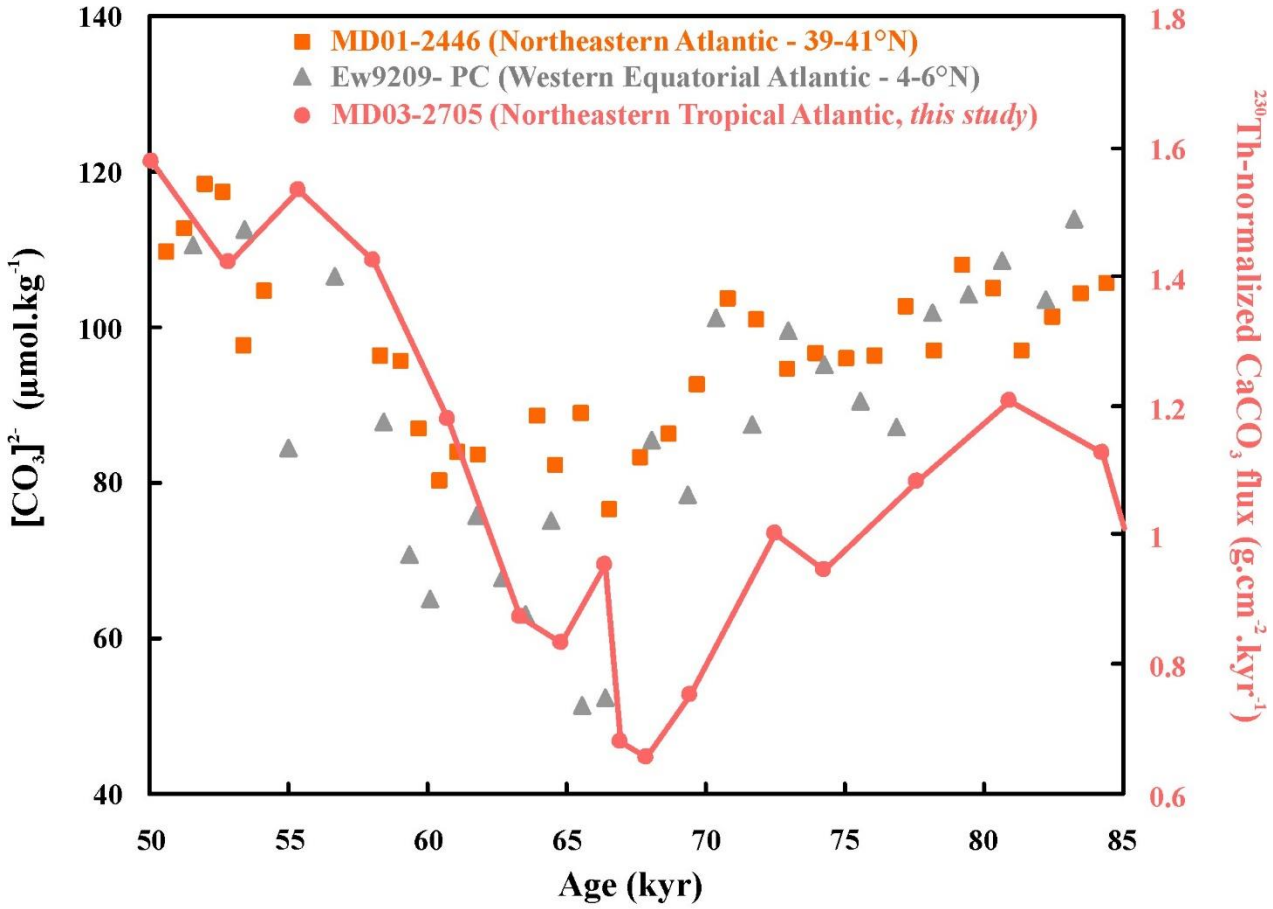

Fig. S5. Comparison between MD03-2705 ^{230}Th-normalized $CaCO_3$ fluxes and reconstructed $[CO_3^{2-}]$ from *Cibicidoides wuellerstorfi* B/Ca between 90 and 50 ka. $CaCO_3$ fluxes at MD03-2705 (pink) are from this study. Carbonate ion concentration reconstructions for northeastern Atlantic (MD01-2446, 3576m water depth, orange squares) and equatorial Atlantic (EW9209-2JPC, 3528m water depth, grey triangles) sites are from (*27*). These sites were chosen because of their high-resolution records and relative proximity to MD03-2705, but other sites in water depths ranging from 3-5 km show similar carbonate ion changes.

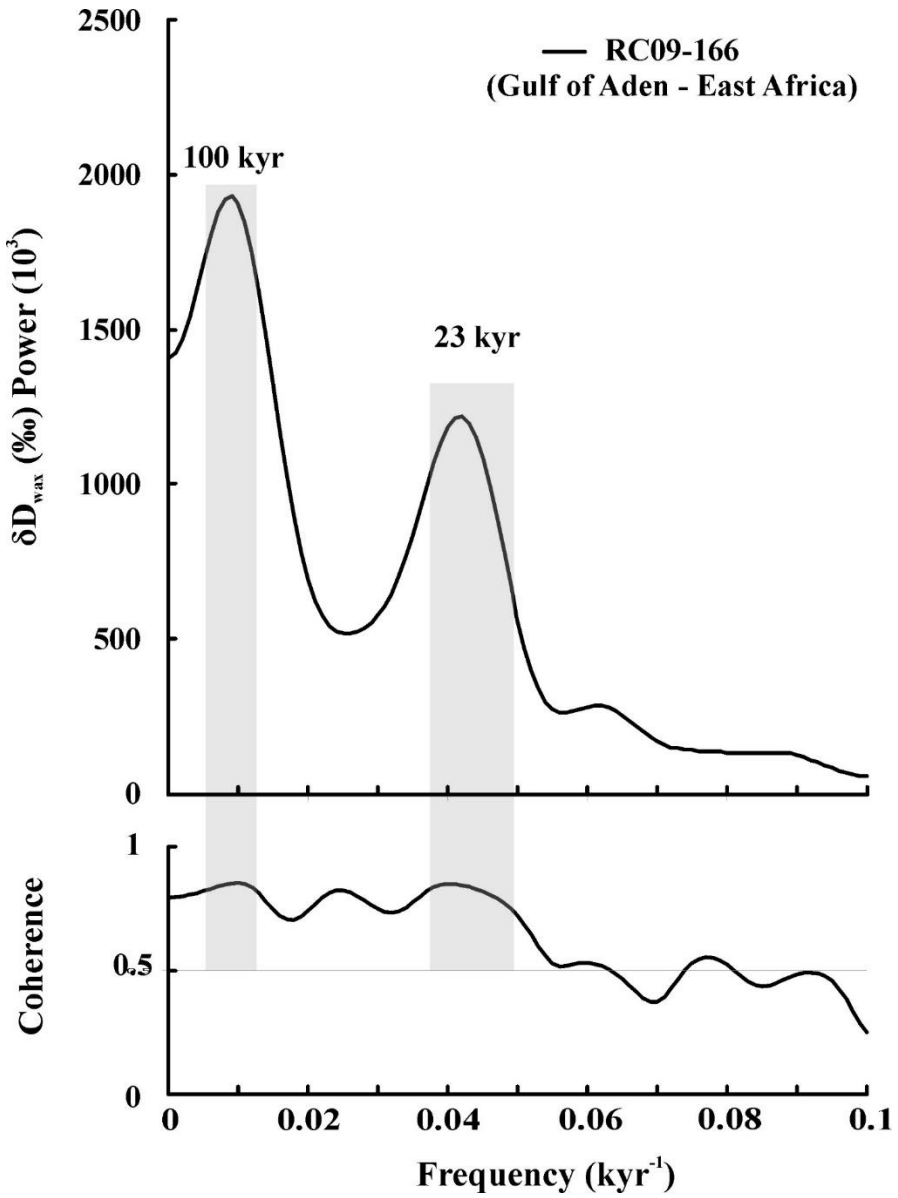

Fig. S6. Power spectral analysis of RC09-166 δ*D*$_{wax}$ (East Africa). While the Gulf of Aden δD_{wax} record (*17*) clearly shows a precessional signal, the spectral analysis of this record also indicates a strong imprint of glacial-interglacial changes. This difference from the MD03-2705 dust record highlights the need for future work to systematically examine the relative importance of glacial-interglacial and precessional variations in different monsoon regions and proxies.

Table S1. Age control points used to build the chronology of the past 240 ka of core MD03-2705. (**A**) Depth [cm], (**B**) AMS-^{14}C age (yr BP), (**C**) Standard error, (**D**) Calibration two sigma range after (*51*) using Calib 6.0 (yr BP), (**E**) Calendar Ages (yr BP), (**F**) Source.

A	B	C	D	E	F
16	4340	20	4079-4452	4266	AMS-^{14}C dating / *this study*
23	5215	20	5285-5574	5430	AMS-^{14}C dating / *this study*
27	7935	20	8097-8398	8248	AMS-^{14}C dating / *this study*
38	10650	70	11308-11962	11635	AMS-^{14}C dating / *from* (*24*)
60	11400	30	12590-12914	12752	AMS-^{14}C dating / *this study*
75	11745	35	12854-13286	13070	AMS-^{14}C dating / *this study*
94	13510	80	15081-16351	15716	AMS-^{14}C dating / *from* (*24*)
107	14595	40	16848-17457	17153	AMS-^{14}C dating / *this study*
119	15750	45	18040-18665	18353	AMS-^{14}C dating / *this study*
135	17130	60	19447-20054	19751	AMS-^{14}C dating / *this study*
142	17240	60	19543-20187	19865	AMS-^{14}C dating / *from* (*24*)
154	19030	70	21577-22363	21970	AMS-^{14}C dating / *this study*
160	20300	100	23201-23978	23590	AMS-^{14}C dating / *from* (*24*)
176	21710	120	24884-25826	25355	AMS-^{14}C dating / *from* (*24*)
198				27000	Isotopic events after (*39*) / *in* (*24*)
296				38090	Isotopic events after (*40*) / *this study*
390				63140	Isotopic events after (*40*) / *this study*
460				73910	Isotopic events after (*40*) / *this study*
495				85550	Isotopic events after (*39*) / *in* (*24*)
505				88030	Isotopic events after (*39*) / *in* (*24*)
630				109000	Isotopic events after (*39*) / *in* (*15*)
695				124000	Isotopic events after (*39*) / *in* (*15*)
725				132500	Isotopic events after (*39*) / *in* (*24*)
760				135000	Isotopic events after (*39*) / *in* (*15*)
860				156000	Isotopic events after (*39*) / *in* (*15*)
970				177000	Isotopic events after (*39*) / *in* (*15*)
1020				192000	Isotopic events after (*39*) / *in* (*15*)
1090				206000	Isotopic events after (*39*) / *in* (*15*)
1140				223000	Isotopic events after (*39*) / *in* (*15*)
1210				238000	Isotopic events after (*39*) / *in* (*15*)
1270				252000	Isotopic events after (*39*) / *in* (*15*)

Table S2. MD03-2705 core depth, model age, thorium and uranium activities, and carbonate content as well as sediment, dust, and carbonate fluxes for the past 240 ka. (**A**) Depth [cm], (**B**) Age model [ka], (**C**) ^{230}Th [dpm/g], (**D**) ^{232}Th [dpm/g], (**E**) ^{238}U [dpm/g], (**F**) excess ^{230}Th [dpm/g], (**G**) $^{238}U_{authigenic}$ [dpm/g], (**H**) Sediment flux [g.cm^{-2}.ka^{-1}], (**I**) dust flux [g.cm^{-2}.ka^{-1}], (**J**) dust flux 1 sigma uncertainty, (**K**) $CaCO_3$ [%], (**L**) $CaCO_3$ flux [g.cm^{-2}.ka^{-1}], (**M**) $CaCO_3$ flux 1 sigma uncertainty. Data in grey are from (*44*). All other data are from this study. No data (n.d.).

A	**B**	**C**	**D**	**E**	**F**	**G**	**H**	**I**	**J**	**K**	**L**	**M**
1	0,38	3,91	0,75	0,02	3,54	0,02	2,33	0,72	0,04	64,55	1,50	0,09
4	1,02	4,68	0,97	0,00	4,20	0,00	1,95	0,77	0,05	68,91	1,34	0,08
8	1,95	4,17	0,83	0,00	3,77	0,00	2,16	0,73	0,04	64,34	1,39	0,08
12	2,97	5,51	0,69	0,00	5,17	0,00	1,55	0,44	0,02	70,06	1,09	0,06
16	4,07	4,79	0,75	0,00	4,43	0,00	1,80	0,55	0,03	64,09	1,15	0,07
20	5,26	5,74	0,73	0,00	5,39	0,00	1,46	0,44	0,02	67,75	0,99	0,06
24	6,55	5,64	0,69	0,01	5,32	0,01	1,46	0,41	0,02	70,75	1,04	0,06
28	7,92	5,25	0,69	0,04	4,93	0,04	1,56	0,44	0,02	75,49	1,18	0,07
30	8,63	4,16	0,78	0,57	3,76	0,18	2,03	0,64	0,04	70,32	1,43	0,08
32	9,37	3,10	0,48	0,16	2,86	0,16	2,65	0,52	0,03	72,02	1,91	0,11
34	10,14	3,14	0,55	0,48	2,84	0,20	2,65	0,60	0,03	75,16	1,99	0,12
36	10,92	2,69	0,75	0,04	2,35	0,04	3,19	0,98	0,06	67,05	2,14	0,14
37	11,32	2,93	0,92	0,60	2,46	0,14	3,03	1,14	0,08	61,55	1,87	0,13
39	11,76	3,03	1,02	0,65	2,50	0,14	2,97	1,24	0,09	59,05	1,75	0,12
40	11,88	2,79	1,06	0,00	2,32	0,00	3,20	1,39	0,10	53,45	1,71	0,12
42	12,08	3,40	1,37	0,80	2,70	0,11	2,74	1,54	0,12	46,68	1,28	0,10
44	12,24	3,38	1,75	0,00	2,61	0,00	2,83	2,02	0,18	32,69	0,93	0,08
46	12,38	3,39	1,77	1,04	2,49	0,16	2,97	2,15	0,20	29,74	0,88	0,08
47	12,44	2,62	0,88	1,64	2,03	1,20	3,63	1,31	0,09	26,20	0,95	0,07
48	12,49	2,97	1,80	0,00	2,18	0,00	3,38	2,50	0,25	25,35	0,86	0,09
50	12,57	3,14	1,73	1,08	2,25	0,22	3,28	2,33	0,23	26,84	0,88	0,09
51	12,60	2,94	1,69	1,03	2,07	0,19	3,56	2,46	0,25	25,87	0,92	0,09
52	12,63	2,16	1,12	0,00	1,67	0,00	4,40	2,01	0,18	26,11	1,15	0,10
56	12,71	2,43	0,67	0,02	2,14	0,02	3,44	0,94	0,06	67,90	2,34	0,15
60	12,75	2,56	0,73	0,00	2,24	0,00	3,28	0,97	0,06	69,04	2,26	0,15
64	12,78	2,44	0,69	0,00	2,14	0,00	3,44	0,97	0,06	68,86	2,37	0,15
68	12,84	2,57	0,75	0,00	2,24	0,00	3,28	1,00	0,06	67,61	2,22	0,14
72	12,94	2,65	0,83	0,00	2,29	0,00	3,20	1,09	0,07	65,26	2,09	0,14
76	13,12	2,51	0,75	0,00	2,18	0,00	3,36	1,03	0,07	67,18	2,25	0,15
80	13,42	2,52	0,68	0,00	2,23	0,00	3,28	0,91	0,06	71,19	2,34	0,15
84	13,85	2,40	0,67	0,01	2,12	0,01	3,44	0,94	0,06	68,83	2,37	0,15

88	14,44	2,93	0,71	0,01	2,62	0,01	2,76	0,80	0,05	71,16	1,97	0,12
92	15,24	2,78	0,62	0,01	2,52	0,01	2,86	0,73	0,04	71,49	2,04	0,12
96	16,05	3,04	0,73	0,00	2,73	0,00	2,61	0,78	0,05	63,96	1,67	0,10
104	17,08	3,52	1,04	0,16	3,06	0,16	2,31	0,98	0,06	54,34	1,25	0,08
108	17,42	3,69	1,08	0,52	3,15	0,52	2,24	0,99	0,07	54,33	1,22	0,08
112	17,69	3,86	1,35	0,98	3,13	0,98	2,24	1,24	0,09	53,24	1,19	0,09
116	17,94	4,37	1,40	1,05	3,61	1,05	1,94	1,11	0,08	52,57	1,02	0,07
120	18,20	4,48	1,47	1,29	3,65	1,29	1,92	1,16	0,08	49,77	0,95	0,07
124	18,48	4,77	1,34	1,17	4,01	1,17	1,74	0,96	0,06	50,20	0,87	0,06
128	18,80	4,44	1,40	1,19	3,66	1,19	1,90	1,09	0,07	51,61	0,98	0,07
132	19,18	4,62	1,33	0,93	3,91	0,93	1,78	0,97	0,06	54,86	0,97	0,06
136	19,61	4,77	1,33	0,96	4,05	0,96	1,71	0,93	0,06	54,82	0,94	0,06
140	20,09	4,58	1,18	0,56	4,00	0,56	1,72	0,83	0,05	54,26	0,93	0,06
144	20,63	4,64	1,29	0,45	4,04	0,45	1,69	0,89	0,06	52,77	0,89	0,06
152	21,83	4,28	1,28	1,06	3,56	1,06	1,90	1,00	0,07	53,39	1,02	0,07
156	22,47	4,45	1,34	0,60	3,79	0,60	1,77	0,97	0,06	50,27	0,89	0,06
160	23,12	4,51	1,10	0,38	4,00	0,38	1,67	0,76	0,05	51,43	0,86	0,05
164	23,76	4,63	1,56	0,34	3,95	0,34	1,68	1,07	0,07	48,32	0,81	0,06
168	24,38	4,50	1,39	0,30	3,89	0,30	1,70	0,97	0,06	50,52	0,86	0,06
172	24,97	4,37	1,18	0,39	3,82	0,39	1,72	0,83	0,05	52,40	0,90	0,06
176	25,50	4,31	1,40	0,14	3,74	0,14	1,75	1,00	0,07	49,45	0,86	0,06
180	25,96	4,32	1,32	0,11	3,80	0,11	1,72	0,93	0,06	53,99	0,93	0,06
181	26,07	4,58	1,27	1,24	3,80	0,61	1,72	0,89	0,06	61,49	1,05	0,07
191	26,82	4,36	1,19	0,83	3,71	0,23	1,74	0,85	0,05	56,04	0,98	0,06
201	27,34	4,02	1,14	0,83	3,39	0,26	1,91	0,89	0,06	57,51	1,10	0,07
211	28,47	3,92	1,05	1,16	3,24	0,64	1,99	0,86	0,06	62,98	1,26	0,08
221	29,60	3,60	0,92	1,15	2,96	0,70	2,18	0,82	0,05	68,25	1,49	0,10
231	30,73	3,39	0,89	1,08	2,78	0,64	2,31	0,84	0,05	67,90	1,57	0,10
241	31,87	3,29	0,91	0,80	2,75	0,34	2,33	0,87	0,06	68,96	1,61	0,11
251	33,00	3,75	0,98	1,61	2,96	1,11	2,15	0,86	0,06	63,34	1,36	0,09
261	34,13	3,40	0,99	1,68	2,58	1,18	2,44	0,99	0,07	61,28	1,50	0,10
271	35,26	3,42	0,91	1,71	2,61	1,26	2,39	0,89	0,06	63,59	1,52	0,10
281	36,39	3,22	0,90	1,47	2,47	1,02	2,49	0,91	0,06	68,33	1,70	0,12
291	37,52	2,84	0,78	1,04	2,25	0,65	2,69	0,86	0,06	65,09	1,75	0,12
301	39,42	2,98	1,32	1,05	2,20	0,39	2,71	1,47	0,13	49,87	1,35	0,12
311	42,09	2,85	1,24	1,02	2,10	0,40	2,80	1,42	0,12	49,68	1,39	0,12
321	44,89	3,12	1,04	1,41	2,29	0,89	2,51	1,07	0,08	59,23	1,49	0,11
325	45,82	3,15	0,67	1,29	2,48	0,95	2,30	0,63	0,04	73,77	1,70	0,11
331	47,42	3,05	0,64	1,15	2,42	0,83	2,32	0,61	0,04	74,28	1,72	0,11
341	50,08	3,20	0,72	1,07	2,58	0,71	2,14	0,63	0,04	73,80	1,58	0,10
351	52,75	2,82	1,06	0,80	2,19	0,27	2,46	1,07	0,08	57,65	1,42	0,11
361	55,41	2,80	0,92	0,67	2,26	0,21	2,33	0,88	0,06	65,87	1,53	0,11
371	58,08	3,05	0,88	0,81	2,45	0,37	2,09	0,75	0,05	68,04	1,42	0,10
381	60,74	3,29	1,12	0,93	2,57	0,37	1,95	0,90	0,07	60,59	1,18	0,09
391	63,37	3,70	1,41	0,98	2,87	0,27	1,70	0,98	0,08	51,42	0,87	0,07
401	64,83	3,79	1,43	0,94	2,97	0,22	1,60	0,94	0,07	52,21	0,83	0,07

411	66,37	3,13	1,27	0,90	2,36	0,26	1,96	1,02	0,08	48,76	0,95	0,08
415	66,99	4,58	1,74	0,89	3,70	0,02	1,24	0,88	0,07	55,09	0,68	0,05
421	67,91	3,95	1,66	0,91	3,08	0,08	1,46	1,00	0,08	44,86	0,66	0,05
431	69,45	3,66	1,52	0,86	2,85	0,10	1,54	0,96	0,08	49,03	0,75	0,06
451	72,53	2,94	1,64	0,90	2,08	0,08	2,01	1,35	0,15	49,87	1,00	0,11
461	74,24	2,78	1,37	0,83	2,01	0,14	2,02	1,14	0,11	46,80	0,95	0,09
471	77,57	2,66	1,37	0,89	1,86	0,20	2,14	1,20	0,12	50,62	1,08	0,11
481	80,89	2,80	0,61	0,79	2,20	0,48	1,76	0,44	0,03	68,42	1,21	0,08
491	84,22	2,97	0,66	0,52	2,52	0,19	1,51	0,41	0,03	74,67	1,13	0,07
495	85,55	2,83	0,84	0,00	2,67	0,00	1,41	0,49	0,03	66,15	0,93	0,06
501	87,04	2,88	0,87	0,53	2,39	0,09	1,56	0,56	0,04	63,14	0,99	0,07
511	89,04	2,86	1,23	0,75	2,16	0,13	1,69	0,85	0,08	48,76	0,82	0,07
521	90,71	2,68	1,12	0,61	2,08	0,05	1,72	0,79	0,07	55,37	0,95	0,08
531	92,39	2,12	0,76	0,51	1,66	0,13	2,12	0,66	0,05	64,81	1,37	0,11
541	94,07	2,10	0,99	0,56	1,56	0,07	2,22	0,90	0,09	62,82	1,39	0,13
551	95,75	2,21	1,05	0,67	1,58	0,15	2,15	0,93	0,09	55,06	1,18	0,12
561	97,42	2,15	1,10	0,87	1,38	0,32	2,42	1,09	0,12	51,07	1,23	0,14
571	99,10	2,52	1,03	0,91	1,74	0,40	1,90	0,80	0,07	55,98	1,06	0,10
581	100,78	2,99	0,93	0,96	2,19	0,50	1,49	0,57	0,04	69,34	1,03	0,08
591	102,46	2,73	0,72	0,64	2,17	0,28	1,48	0,44	0,03	74,12	1,09	0,08
601	104,13	2,31	0,62	0,58	1,82	0,26	1,74	0,44	0,03	77,16	1,34	0,09
611	105,81	2,54	0,94	0,57	2,00	0,09	1,56	0,60	0,05	68,04	1,06	0,09
621	107,49	2,49	1,22	0,71	1,81	0,10	1,71	0,85	0,09	59,21	1,01	0,10
631	109,23	2,62	1,68	1,14	1,57	0,29	1,93	1,33	0,19	51,10	0,99	0,14
641	111,54	2,89	1,96	1,62	1,45	0,64	2,06	1,66	0,30	48,75	1,01	0,18
651	113,85	2,18	1,30	0,82	1,41	0,17	2,09	1,11	0,14	56,78	1,19	0,15
661	116,15	2,18	1,33	0,95	1,30	0,29	2,19	1,21	0,12	48,95	1,09	0,14
671	118,46	2,10	1,40	1,08	1,12	0,38	2,47	1,32	0,13	50,21	1,27	0,17
681	120,77	2,34	1,12	0,87	1,54	0,31	1,79	0,82	0,09	59,37	1,06	0,12
691	123,08	2,78	0,72	0,78	2,09	0,43	1,28	0,38	0,03	72,55	0,93	0,29
701	125,70	2,26	0,53	0,74	1,63	0,47	1,60	0,35	0,02	79,93	1,28	0,20
711	128,53	2,33	0,71	0,77	1,66	0,41	1,55	0,45	0,04	73,07	1,13	0,17
721	131,37	1,79	0,77	0,80	1,08	0,42	2,33	0,74	0,08	69,49	1,62	0,13
731	132,93	2,55	0,84	1,66	1,15	1,25	2,15	0,74	0,09	67,82	1,46	0,12
741	133,64	2,89	0,93	2,04	1,18	1,57	2,06	0,78	0,10	62,96	1,29	0,07
751	134,36	2,67	1,01	1,94	1,03	1,43	2,31	0,95	0,10	57,02	1,33	0,09
761	135,21	4,16	1,13	3,21	1,48	2,64	1,59	0,74	0,09	58,54	0,93	0,09
771	137,31	3,71	1,07	2,81	1,35	2,28	1,72	0,75	0,10	57,58	0,99	0,08
781	139,41	3,51	1,26	2,63	1,27	2,00	1,80	0,93	0,14	54,03	0,97	0,09
791	141,51	2,95	1,09	2,02	1,21	1,47	1,85	0,83	0,11	58,45	1,08	0,18
801	143,61	2,89	1,38	1,71	1,36	1,02	1,62	0,92	0,14	55,20	0,89	0,17
811	145,71	2,59	1,26	1,49	1,25	0,86	1,74	0,90	0,13	56,07	0,97	0,16
821	147,81	2,59	1,43	1,23	1,45	0,51	1,47	0,86	0,12	50,53	0,74	0,22
831	149,91	2,44	1,36	1,07	1,44	0,38	1,46	0,81	0,11	51,32	0,75	0,18
841	152,01	2,08	1,23	1,07	1,09	0,45	1,89	0,96	0,11	48,11	0,91	0,15
851	154,11	2,58	1,45	1,06	1,58	0,34	1,28	0,76	0,10	44,78	0,58	0,12

861	156,19	2,45	1,36	1,03	1,47	0,35	1,36	0,75	0,10	47,72	0,65	0,13
871	158,10	2,19	1,39	1,03	1,21	0,34	1,61	0,91	0,15	46,84	0,75	0,15
881	160,01	2,25	1,48	1,18	1,14	0,44	1,69	1,02	0,19	48,93	0,83	0,15
891	161,92	2,15	1,56	1,15	1,05	0,37	1,79	1,15	0,24	43,56	0,78	0,13
901	163,83	2,33	1,61	1,32	1,08	0,52	1,64	1,12	0,17	43,44	0,76	0,14
911	165,74	2,00	1,68	1,38	0,69	0,54	2,64	1,81	0,43	31,76	0,84	0,11
921	167,65	2,77	1,30	1,79	1,12	1,14	1,52	0,83	0,10	31,76	0,51	0,10
926	168,60	3,70	1,30	2,40	1,53	1,75	1,16	0,61	0,08	55,08	0,64	0,15
931	169,55	4,05	0,86	2,66	1,67	2,23	1,05	0,37	0,04	71,56	0,75	0,14
941	171,46	2,81	0,83	1,74	1,23	1,33	1,39	0,47	0,05	70,90	0,99	0,11
951	173,37	2,09	0,70	1,42	0,79	1,06	2,08	0,60	0,06	74,65	1,59	0,08
961	175,28	2,07	1,09	1,05	1,07	0,51	1,53	0,69	0,10	68,19	1,04	0,09
991	183,30	1,93	1,12	1,51	0,52	0,95	2,85	1,30	0,28	54,14	1,63	0,12
1011	189,30	2,28	1,20	1,39	0,96	0,79	1,54	0,76	0,14	54,39	0,84	0,15
1021	192,20	1,93	1,84	1,04	0,90	0,12	1,61	1,21	0,35	40,47	0,65	0,16
1031	194,20	1,71	1,09	1,04	0,71	0,49	1,98	0,88	0,20	58,75	1,16	0,13
1040	196,00	3,40	1,03	0,85	2,57	0,34	0,54	0,23	0,02	63,44	0,34	0,20
1051	198,20	2,07	0,98	0,98	1,12	0,49	1,20	0,48	0,06	60,08	0,72	0,12
1061	200,20	1,55	0,93	0,60	0,96	0,14	1,37	0,52	0,08	67,52	0,92	0,28
1071	202,20	1,23	1,09	0,68	0,56	0,14	2,31	1,03	0,29	59,79	1,38	0,28
1081	204,20	1,38	1,07	0,56	0,82	0,02	1,52	0,67	0,13	62,87	0,96	0,20
1091	206,34	1,20	1,24	0,60	0,61	-0,02	2,02	1,02	0,29	56,75	1,14	0,07
1101	209,74	1,29	1,34	0,66	0,63	-0,01	1,90	1,04	0,31	50,92	0,97	0,11
1111	213,14	1,28	0,85	0,77	0,54	0,34	2,18	0,76	0,17	69,45	1,51	0,07
1121	216,54	1,42	0,54	0,95	0,50	0,68	2,25	0,50	0,08	78,11	1,76	0,09
1131	219,94	1,40	0,65	0,78	0,65	0,46	1,72	0,46	0,07	75,88	1,31	0,08
1141	223,21	2,41	1,14	1,23	1,21	0,66	0,89	0,42	0,06	61,31	0,55	0,11
1151	225,36	1,88	1,33	1,57	0,35	0,91	2,88	1,51	0,58	48,75	1,51	0,26
1155	226,21	1,87	1,24	1,29	0,40	0,76	2,64	1,29	0,40	53,83	1,43	0,20
1161	227,50	1,96	1,46	1,27	0,40	0,69	2,59	1,55	0,63	53,43	1,38	0,17
1171	229,64	1,72	1,51	1,14	0,59	0,38	1,70	1,06	0,39	50,63	0,86	0,16
1181	231,79	1,79	1,28	1,45	0,37	0,81	2,47	1,30	0,46	49,55	1,37	0,64
1191	233,93	2,43	1,16	1,70	0,76	1,12	1,27	0,60	0,14	55,56	0,71	0,40
1201	236,07	2,66	0,65	1,95	0,76	1,63	1,25	0,33	0,05	73,38	0,91	0,36
1221	240,57	1,61	0,81	1,22	0,41	0,81	2,22	0,74	0,22	n.d.	n.d.	n.d.